Short Note

Angle-domain parameters computed via weighted slant-stack

Claudio Guerra

INTRODUCTION

It is well known that angle-domain common-image gathers (ADCIGs) in geologically complex regions can show undesirable kinematic effects and amplitude variations along the angle axis due to illumination problems (Prucha et al., 2000; Valenciano, 2006). The subsurface-offset-to-angle transformation includes some regularization of the linear interpolation problem (Prucha et al., 2000; Sava and Fomel, 2000) along the angle axis which, to some extent diminishes the amplitude variations not related to the interpolation problem. However, the correct solution to the amplitude variation problem is achieved by computing a least-squares inverse image (Clapp, 2005). The inverse problem can be solved either iteratively by applying the migration operator and its transpose in every iteration, or according to the approach proposed by Valenciano (2006), in which the Hessian is computed in a target-oriented way and solved iteratively as an inversion problem. This problem can be solved either in the subsurface-offset domain or in the reflection-angle domain.

To solve the inversion problem in the reflection-angle domain it should be computed the angle-domain Hessian. Alternatively, the angle-domain Hessian can be evaluated by chaining the offset-to-angle operator and the subsurface-offset Hessian (Valenciano and Biondi, 2005). Valenciano and Biondi (2007) proposed to obtain the angle-domain Hessian by applying the slant-stack technique to compute ADCIGs on the subsurface-offset Hessian. They noticed that the resulting angle-domain Hessian for a model with a Gaussian velocity anomaly lacked the resolution to determine which angles were more illuminated. Recently, Fomel (2003) introduced the theoretical framework of the oriented wave equation, under which computing the angle-domain Hessian can be promising.

Here, I propose a general framework to map any information computed in the subsurface-offset domain to the angle-domain. The proposed approach relies on the asymptotic nature of the slant-stack transformation from subsurface-offset to angle domain. I first show the validity of the stationary-phase assumption for the offset-to-angle transformation, then describe the weighted transformation from subsurface-offset to reflection-angle domain, and finally illustrate the technique with the transformation of the diagonal of the Hessian in the subsurface-offset domain to the angle domain, yielding amplitude factors to compensate for illumination problems in ADCIGs. Additionally, I show the transformation of some off-diagonal terms

which, at present, does not have a direct application in the amplitude correction problem.

PHASE BEHAVIOR OF THE OFFSET-TO-ANGLE TRANSFORMATION

The offset-to-angle transformation can be expressed by the integration of the SODCIG, $P(z,h)$, along a certain slanted path, according to the equation

$$Q(z,\gamma) = \int_A \varrho[P(z,h)]dh|_{z=\zeta(\gamma,h)}, \tag{1}$$

where $Q(z,\gamma)$ is the output ADCIG, γ is the aperture angle, h is the subsurface offset, ϱ is the *rho*-filter which aims to yield the correct phase of the output ADCIG (Claerbout, 1997), A is the domain of integration that defines the range of subsurface offsets to be summed, and $\zeta(\gamma,h)$ is the slanted path given by

$$\zeta(\gamma,h) = z_0 + h\tan\gamma, \tag{2}$$

where z_0 is the depth coordinate at zero subsurface offset. A single reflector in a SODCIG can be represented by

$$P(z,h) = A(h)f(z - z_r(h)), \tag{3}$$

where $A(h)$ is an amplitude term whose value depends on the reflection coefficient, illumination and focusing, f is the seismic pulse, and z_r is the reflector depth. The fact that A and z_r are functions of h accommodates reflector amplitudes being focused at nonzero-subsurface offsets because of inaccuracies in migration velocity and problems in illumination. A SODCIG containing several reflectors can be described by the superposition of individual reflectors like that described by equation 3.

Equation 1, Fourier transformed to the k_z domain after inserting equation 3, reads

$$\hat{Q}(k_z,\gamma) = \sqrt{\frac{-ik_z}{2\pi}}F(k_z)\int_{-h}^{h} A(h)e^{-ik_z\Phi(\gamma,h)}dh, \tag{4}$$

where $\Phi(\gamma,h) = \zeta(\gamma,h) - z_r(h)$ is the phase function. Assuming that $A(h)$ is not itself an oscillating function, and considering the high-k_z regime, the argument of the integral in equation 4 rapidly oscillates, yielding negligible amplitudes for integration over a full period, except for the case where the phase function, $\Phi(\gamma,h)$, remains stationary. This condition is achieved in the vicinity of a point – the stationary point – in the SODCIG with a certain subsurface offset, $h^\star$, where $\zeta(\gamma,h)$ is tangent to $z_r(h)$, or

$$\begin{aligned} \zeta(\gamma,h) &= z_r(h) \\ \frac{\partial\zeta(\gamma,h)}{\partial h} &= \frac{\partial z_r(h)}{\partial h}, \end{aligned}$$

estimated in $h = h^\star$.

Equation 4 can be evaluated by the stationary-phase method. According to Bleistein (1984), under the assumption of a single stationary point in which the second derivative does not vanish, integrals like

$$I(\lambda) = \int_A f(t) e^{i\lambda\phi(t)} dt, \tag{5}$$

where $f(t)$ is a smooth and compact function, can be asymptotically approximated by

$$I(\lambda) \sim e^{i(\lambda\phi(c) + sgn(\phi''(c))\frac{\pi}{4})} f(c) \sqrt{\frac{2\pi}{\lambda\,|\phi''(c)|}}, \tag{6}$$

if $\lambda \to \infty$. The term $sgn(\phi''(c))$ corresponds to the signal of second derivative of the phase function, $\phi(t)$, evaluated at the stationary point, c.

It turns out that the stationary phase formula of equation 4 is given by

$$\hat{Q}(k_z, \gamma) \sim \frac{A(h^\star)}{\sqrt{|\Phi''(h^\star)|}} F(k_z) e^{-ik_z \Phi(\gamma, h^\star)}. \tag{7}$$

Finally, the inverse Fourier transform of equation 7 gives

$$Q(z, \gamma) \sim \frac{A(h^\star)}{\sqrt{|\Phi''(h^\star)|}} F(z - \Phi(\gamma, h^\star)). \tag{8}$$

Equation 8 shows that the main contribution to the amplitudes in the ADCIG comes from the vicinity of the stationary point. The second derivative of the phase function with respect to h is basically the second derivative of z_r, as $\zeta(\gamma, h)$ is a straight line. If z_r is a straight event in the SODCIG, meaning that just a very small range of angles has been illuminated, as in the case of a single shot and well-sampled receiver wavefield as discussed by Tang (2007), there will be as many stationary points as subsurface offsets. In this situation, the integration interval is divided in such a way that each new interval contains only one stationary point, and the final result is the sum of all individual stationary-points contribution. The other special case is when all the energy is focused at zero subsurface-offset, indicating good illumination for all reflection angles and migration with the correct velocity. It is a generalization of the previous case and is solved in the same way for various illumination angles.

WEIGHTED OFFSET-TO-ANGLE TRANSFORMATION

Bleistein (1987) describes a strategy to estimate parameters from the subsurface using different images migrated with two slightly different weights. Tygel et al. (1993) applied the same ideas to what they called a multiple-weight diffraction stack to obtain the stationary point location that in turn, along with source and receiver position, specifies the reflection ray. For instance, if one desires to estimate reflector dips, a possible way to do that is by computing two different migrated images, M_a and M_1 obtained with two distinct migration-weighting functions, say the migration angle (M_a result) and simply a constant value of one (M_1 result). For M_a, the resulting amplitudes are weighted by the migration angles around the stationary point. As in

this region the migration operator and reflectors are tangent, the average of the migration angle is an estimate of the reflector dip. So, the division M_a/M_1 results in an estimate of the dip of the reflectors.

After analyzing the phase behavior of the offset-to-angle transformation in the previous section and taking into account that the main contribution for the image in the angle domain comes from the vicinity where the phase function remains stationary in the subsurface offset domain, the use of the weighted stacking strategy (Bleistein, 1987) to map quantities computed in the subsurface-offset domain to the angle domain is straightforward. The mapping of certain attributes can be useful, for instance, to balance amplitudes in the angle domain.

In the following, the aim of the weighted offset-to-angle transformation is to compute weights to be applied on ADCIGs in such a way that amplitude variations due to illumination problems are attenuated. The weighted offset-to-angle transformation is represented by the computation of ADCIGs from SODCIGs previously multiplied by some parameter – in the present case, the subsurface-offset Hessian diagonals – defined in the subsurface-offset domain. These ADCIGs are to be divided by the non-weighted transformed results, using a regularization term to avoid division by small numbers. Finally, a median filter is applied to remove spurious amplitudes, thus providing an estimate of that parameter in the transformed domain.

The general formula of the Hessian in the prestack-inversion problem is

$$\mathbf{H}(\mathbf{x},\mathbf{h};\mathbf{x}',\mathbf{h}') = \sum_{\omega}\sum_{\mathbf{x_s}} \mathbf{G_s^*}(\mathbf{x}+\mathbf{h},\mathbf{x_s};\omega)\mathbf{G_s}(\mathbf{x}'+\mathbf{h}',\mathbf{x_s};\omega)\sum_{\mathbf{x_r}} \mathbf{G_r^*}(\mathbf{x}-\mathbf{h},\mathbf{x_r};\omega)\mathbf{G_r}(\mathbf{x}'-\mathbf{h}',\mathbf{x_r};\omega) \tag{9}$$

where G_s denotes Green's function from source point, $\mathbf{x_s}$, to the image point, $\mathbf{x}$, and G_r the Green's function from the image point to the receiver point, $\mathbf{x_r}$, $\mathbf{h}$ is the subsurface-offset, the prime indicates points in the image space in the vicinity of the image point and different subsurface-offsets, and the * stands for the conjugate transpose of the Green's functions. The main diagonal of the Hessian, which is the Laplacian of the cost function related to the model parameters, contains the autocorrelation of the Green's functions and, generally, carries most of the information about the illumination. Sometimes, a good and cheap solution is just to approximate the Hessian by its main diagonal and apply its inverse to the migrated image. But, this procedure does not correct for kinematic errors of the migrated image and, depending on the complexity of the illumination pattern, only the least-squares inverse image can provide reasonable results (Clapp, 2005).

Equation 10 shows the structure of the subsurface-offset domain Hessian used in the examples.

$$\mathbf{H}(\mathbf{x},\mathbf{h};\mathbf{h}') = \sum_{\omega}\sum_{\mathbf{x_s}} \mathbf{G_s^*}(\mathbf{x}+\mathbf{h},\mathbf{x_s};\omega)\mathbf{G_s}(\mathbf{x}+\mathbf{h}',\mathbf{x_s};\omega)\sum_{\mathbf{x_r}} \mathbf{G_r^*}(\mathbf{x}-\mathbf{h},\mathbf{x_r};\omega)\mathbf{G_r}(\mathbf{x}-\mathbf{h}',\mathbf{x_r};\omega) \tag{10}$$

As one can notice, the diagonals represent just the cross-correlation between Green's functions computed at the same image point for different subsurface-offsets. Although, in principle, any diagonal of the subsurface-offset Hessian of such a strucuture can be transformed to the angle

domain by the proposed approach, at present I have conceived a direct application only for the transformed main diagonal.

In the next section I show examples of the angle-domain transformed subsurface-offset Hessian diagonals, as well as the comparison of migrated images before and after the amplitude compensation with the transformed main diagonal, for a small portion of the Sigsbee dataset.

EXAMPLES

The Sigsbee synthetic dataset was used in this work. This well known dataset presents illumination problems due to an irregular salt body shape which manifest as unbalanced amplitude patterns in the seismic section. The small rectangle in Figure 1 highlights the target area. The off-end acquisition geometry consists of 348 receivers, 75 ft apart, resulting in 26025 ft maximum offset. As source coordinates are lower than receiver coordinates, the source-receiver offsets are positive. Therefore, the energy will be mainly distributed at positive reflection angles.

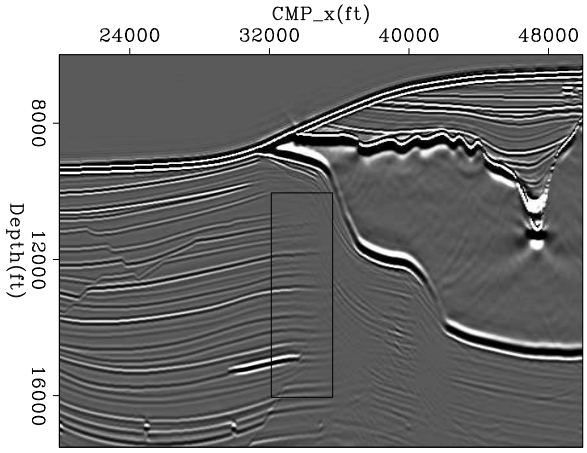

Figure 1: Shot profile migration of part of Sigsbee dataset – zero-subsurface offset. The small box highlights the target area. Sigsbee [ER]

Figures 2 and 3 show two different SODCIGs and their respective subsurface-offset Hessian main diagonal, located at CMP coordinates 33200 ft and 35500 ft, respectively. The lower CMP position is closer to the tip of the salt, and the higher is closer to the salt body. In this work, all figures related to illumination show high-illumination values in dark gray and low illumination values in light gray. Both SODCIGs clearly exhibt the effects of poor illumination represented by horizontal and dipping ($\approx 40^\circ$ – 50°) straight events. The energy smeared along these directions will be mapped to the reflection-angle domain according the dips observed in the subsurface-offset domain. In the SODCIG at CMP position 35500 ft, events curving upward are the expression of internal multiples reflecting at the top and base of the salt body.

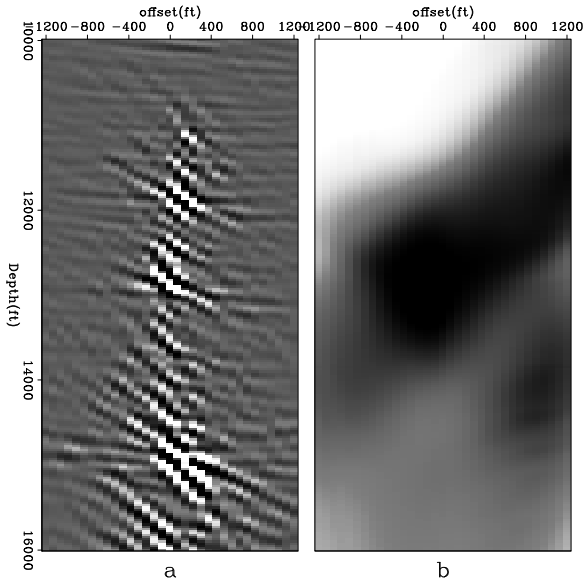

Figure 2: SODCIG and diagonal of the subsurface-offset Hessian at CMP coordinate 33200 ft. Note the effects of poor illumination represented by horizontal and dipping straight events in the SODCIG. Ojoin16 [ER]

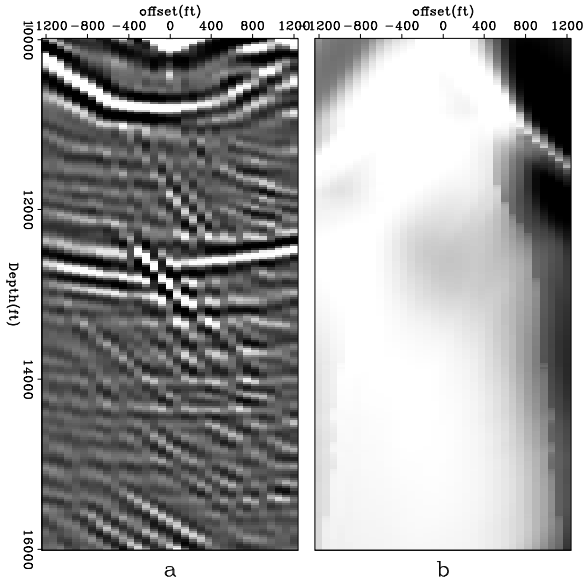

Figure 3: SODCIG and diagonal of the subsurface-offset Hessian at CMP coordinate 33200 ft. Upward curved events correspond to internal multiples reflecting at the top and base of the salt body. Note the effects of poor illumination represented by horizontal and dipping straight events in the SODCIG. Ojoin50 [ER]

As already predicted, the ADCIGs at CMP coordinates 33200 ft and 35500 ft show focusing of energy at reflection angles around 0° and 40° – 50°, as can be seen in Figures 4 and 5. Additionally, these figures show the original reflection-angle gather (a), the main diagonal of the Hessian transformed to the reflection-angle domain (b), and the amplitude compensated ADCIG (c). Notice how the amplitudes are better distributed along the reflection-angle axis after compensation by the inverse of the diagonal of the Hessian. However, as just the diagonal of the Hessian is being used, the kinematic artifacts remain.

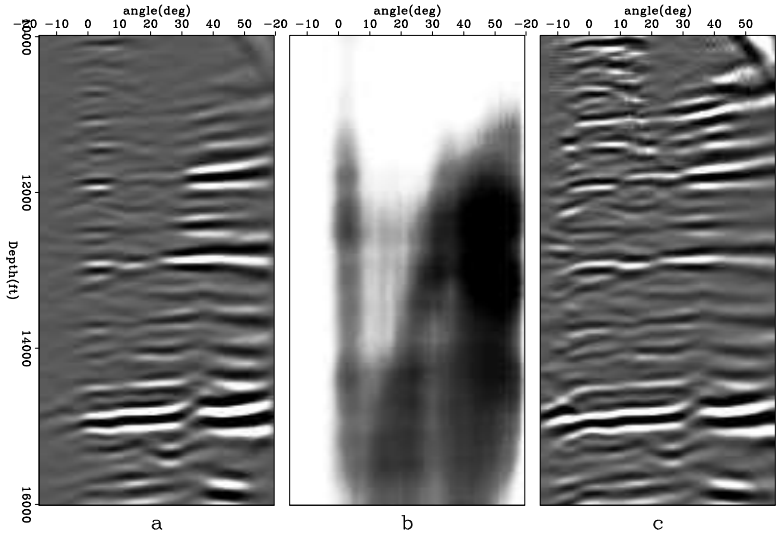

Figure 4: ADCIGs and diagonal of the transformed angle-domain Hessian at CMP coordinate 33200 ft. Before amplitude compensation (a); diagonal of the Hessian in the angle domain (b); and after amplitude compensation (c). Note how much better balanced the amplitude is in the angle direction. join16 [ER]

The proposed approach seems to be dependent on the amplitude strength of the events in the ADCIGs. However, as can be seen in the next example, it yields useful information about illumination. Figures 6, 7 and 8 show angle sections of the original angle data (a), the main diagonal of the Hessian in the angle domain (b) and the amplitude-balanced angle data (c). Again, the amplitude compensation proved to be effective. However, notice how for the zero-angle section the illumination computed in the angle domain is low at the right part of the section, in spite of the high amplitudes of the internal multiples. This confirms, to some extent, that the proposed approach can yield reliable information about illumination even though high amplitudes of events not predicted in the computation of the Green's functions are present.

Figures 9 shows the stacked section along the angle axis, before (a) and after (b) the amplitude compensation by the inverse of the diagonal of the Hessian in the angle domain. The dimming of the amplitudes at the right portion of the section is almost eliminated. However, unfortunately, the amplitudes of internal multiples are increased too.

In the last example, I show, for the zero-angle section, off-diagonal terms after the transformation to the angle domain. In Figure 10 it is clear that off-diagonal terms start gaining importance as we approach the flank of the salt body at the right of the section.

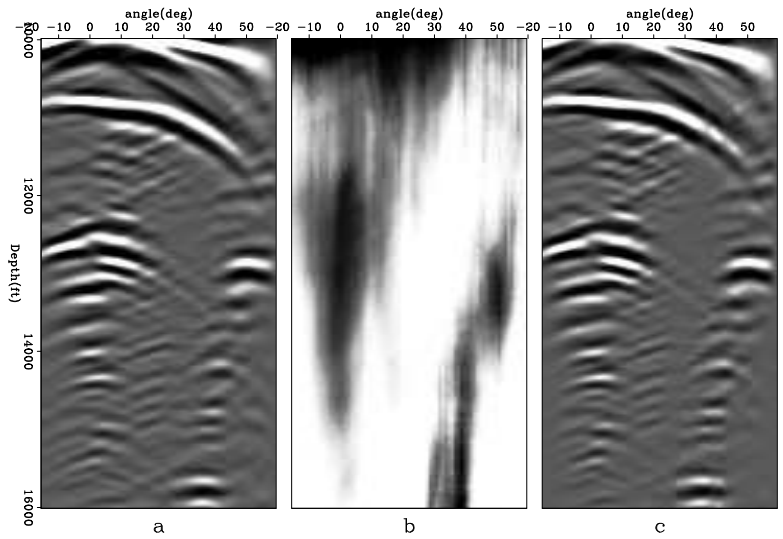

Figure 5: ADCIGs and diagonal of the transformed angle-domain Hessian at CMP coordinate 35500 ft. Before amplitude compensation (a); diagonal of the Hessian in the angle domain (b); and after amplitude compensation (c). join50 [ER]

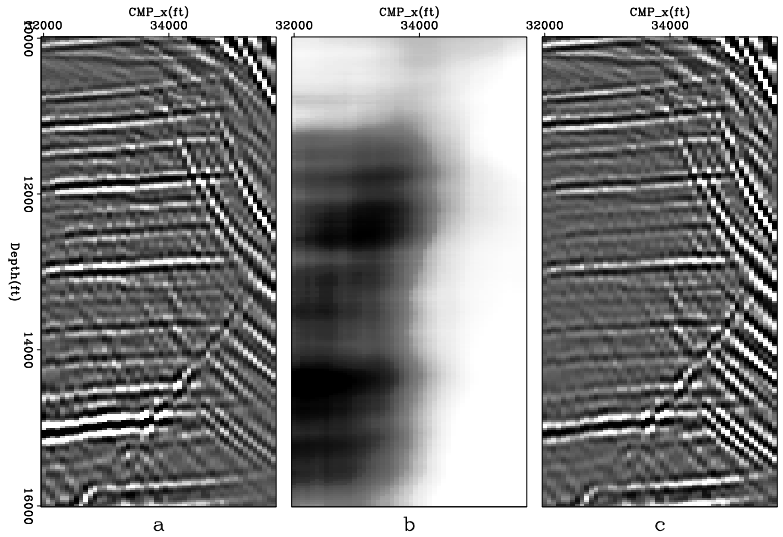

Figure 6: Zero-angle section. Before amplitude compensation (a); diagonal of the Hessian in the angle domain (b); and after amplitude compensation (c). Notice the low illumination in the right part of the section, near the flank of the salt body. join00 [ER]

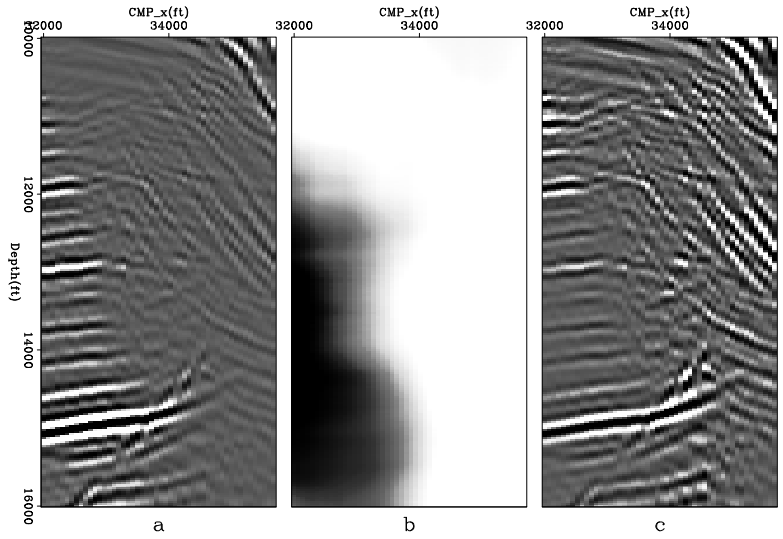

Figure 7: 15°-angle section. Before amplitude compensation (a); diagonal of the Hessian in the angle domain (b); and after amplitude compensation (c). Notice how much better balanced the amplitude is along the CMP direction. join15 [ER]

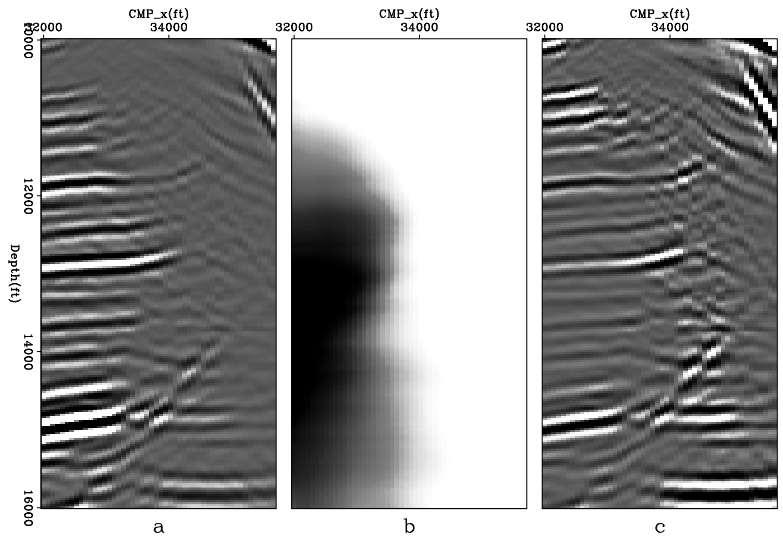

Figure 8: 30°-angle section. Before amplitude compensation (a); diagonal of the Hessian in the angle domain (b); and after amplitude compensation (c). join30 [ER]

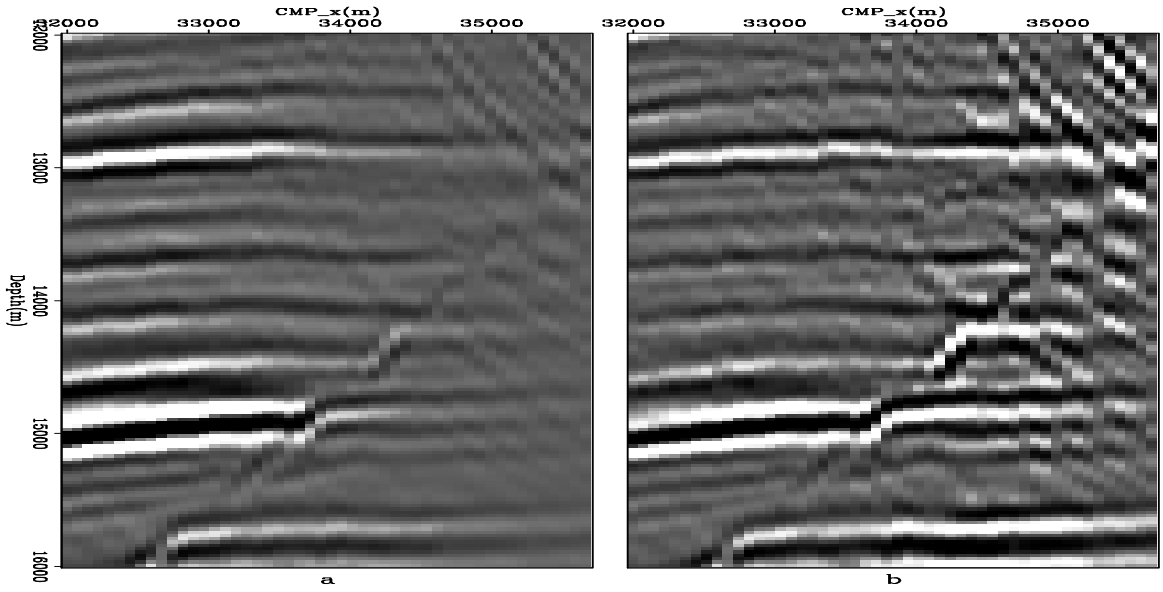

Figure 9: Stack along the angle axis. Before amplitude compensation (a) and after (b). Stk [ER]

CONCLUSIONS

I showed how to estimate angle-domain parameters from the subsurface-offset domain using what I call weighted offset-to-angle, particularly subsurface-offset Hessian diagonals. The proposed approach provides useful information, which can be confirmed by the amplitude compensation results. The transformation of off-diagonal terms of the subsurface-offset Hessian indicates that the results are not strongly dependent on the amplitude distribution in the ADCIGs. However, it is still not clear how to use these transformed off-diagonal terms in inversion schemes.

AKNOWLEDGEMENTS

I would like to thank Alejandro Valenciano for providing me the subsurface-offset domain Hessian and common-image gathers and for the explanations and fruitful discussions.

REFERENCES

Bleistein, N., 1984, Mathematical methods for wave phenomena: Academic Press Inc.

Bleistein, N., 1987, On the imaging of reflectors in the earth: Geophysics, **52**, no. 7, 931–942.

Claerbout, J., 1997, Imaging the earth's interior: `http://sepwww.stanford.edu/sep/prof/toc_html/iei.`

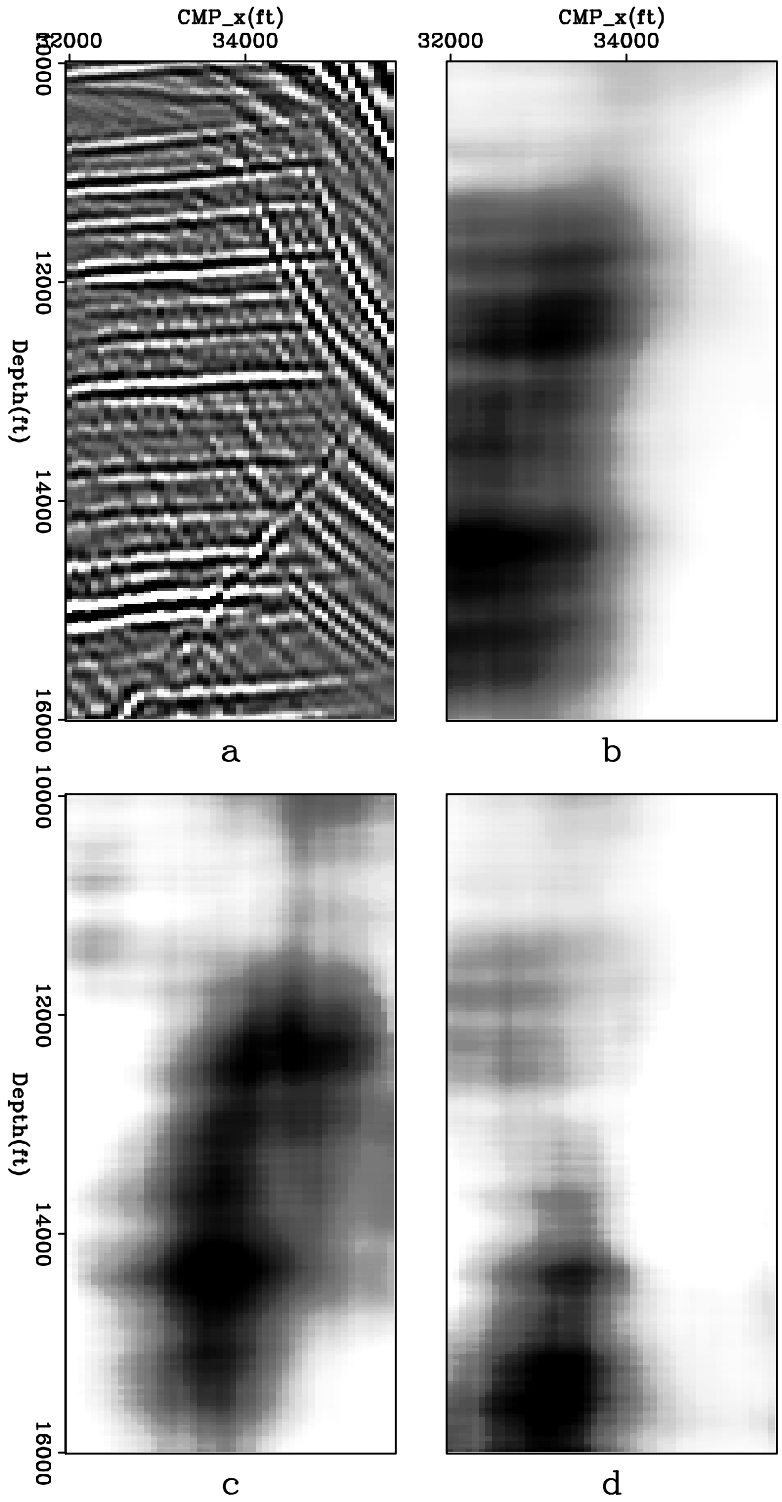

Figure 10: Zero-angle section (a); main diagonal (b); 5th subsurface-offset domain off-diagonal transformed to angle (c); and 15th subsurface-offset domain off-diagonal transformed to angle (d). jDoff01 [ER]

Clapp, M. L., 2005, Imaging under salt: illumination compensation by regularized inversion: Ph.D. thesis, Stanford University.

Fomel, S., 2003, Angle-domain seismic imaging and the oriented wave equation: 73nd Ann. Internat. Mtg, Soc. Expl. Geophys., Expanded Abstracts, pages 893–896.

Prucha, M. L., R. G. Clapp, and B. Biondi, 2000, Seismic image regularization in the reflection angle domain: SEP–**103**, 109–119.

Sava, P. and S. Fomel, 2000, Angle-gathers by Fourier Transform: SEP–**103**, 119–130.

Tang, Y., 2007, Selective stacking in the reflection-angle and azimuth domain: SEP-129, pages 159–178.

Tygel, M., J. Schleicher, P. Hubral, and C. Hanitzsch, 1993, Multiple weights in diffraction stack migration: Geophysics, **59**, no. 12, 1820–1830.

Valenciano, A. A. and B. Biondi, 2005, Wave-equation angle-domain hessian: SEP–**123**.

Valenciano, A. A. and B. Biondi, 2007, Wave-equation inversion prestack hessian: SEP-125, pages 201–209.

Valenciano, A. A., 2006, Target-oriented wave-equation inversion with regularization in the subsurface offset domain: SEP–**124**.